Asociación Argentina
de Mecánica Computacional

Mecánica Computacional Vol XXX, págs. 1143-1158 (artículo completo)
Oscar Möller, Javier W. Signorelli, Mario A. Storti (Eds.)
Rosario, Argentina, 1-4 Noviembre 2011

A REDUCED ORDER MODEL OF A 3D CABLE USING PROPER ORTHOGONAL DECOMPOSITION

Mario R. Escalante[a,b], Rubens Sampaio[c], Marta B. Rosales[d,e] and Thiago Ritto[f]

[a]*FRCU,Universidad Tecnológica Nacional, Ing. Pereyra 676, 3260 C. del Uruguay (ER), Argentina, escalam@frcu.utn.edu.ar*

[b]*FRCon,Universidad Tecnológica Nacional, Salta 277, 3200 Concordia (ER), Argentina*

[c]*Dept. of Mechanical Engineering, PUC-Rio,Rua Marquês de São Vicente 225, 22453-900 Rio de Janeiro, Brasil, rsampaio@puc-rio.br*

[d]*Dpto. de Ingeniería,Universidad Nacional del Sur, Av.Além 1253, 8000 Bahía Blanca, Argentina,mrosales@criba.edu.ar*

[e]*CONICET, Argentina*

[f]*Departamento de Engenharia Mecânica, Universidade Federal do Rio de Janeiro (UFRJ) Cidade Universitária - Ilha do Fundão, 21945-970 Rio de Janeiro, Brasil.*

Keywords: Dynamics of Cables, Proper Orthogonal Decomposition, Model Reduction.

Abstract. Cables and flexible pipes are found in many applications of civil, aerospace, and mechanical engineering. Many offshore engineering problems involve slender rods or cables (pipelines, risers and mooring lines) and also are commonly used in robotics to bring energy to the actuators of a robotic arm. Risers are used, for example, to convey fluids from the bottom of the sea up to the surface. Engineers need numerical models of nonlinear thin deformable structures in order to predict their dynamics and the internal stresses. To accurately simulate the motion of slack marine cables, it is necessary to capture the effects of the cables bending and torsional stiffness. Hence, the need for numerical nonlinear models is still an intense subject of research. In this work, a finite element simulation of cables is used to get a reduced order model by means of the Proper Orthogonal Decompositions (POD). The finite element cable model adopted makes use of a twisted cubic spline element with a lumped mass approximation; it provides a representation of both the bending and torsional effects. Cables are modeled as slender flexible rods that can support environmental, gravitational, and buoyancy forces. The nonlinear equations of motion for the continuous cable are developed in terms of an inertial frame of reference using the Frenet equations. The model permits large deflections and finite rotations and accounts for tension variation along its length as well as nonlinearities arising from applied loads or constraints. The proper orthogonal modes, in conjunction with the Galerkin approach, permit the construction of a lower-dimensional model that is very efficient with respect to the ones constructed with the typical finite elements basis. Different proper orthogonal modes computed from time-series at different excitation frequencies are used and different approximations are compared.

1 INTRODUCTION

In many fields of science and engineering, like fluid or structural mechanics and electric circuit design, large-scale dynamical systems need to be simulated, optimized or controlled. They are often given by discretizations of systems of nonlinear partial differential equations yielding high-dimensional discrete phase spaces. For this reason, during the last decades, research was mainly focused on the development of sophisticated analytical and numerical tools to understand the overall system behavior. Not surprisingly, the number of degrees of freedom for simulations kept pace with the increasing computing power. But, when it comes to optimal design or control the problems, such numerical models are too large to be tackled with standard techniques. Hence, there is a strong need for model reduction techniques to reduce the computational costs and storage requirements. Low-dimensional approximations for the full high-dimensional dynamical system, which reproduce the characteristic dynamics of the system, are desirable.

In this work, a finite element simulation of cables is adopted to obtain a reduced order model by means of the projection method using Proper Orthogonal Decompositions (POD). A twisted cubic spline element form and a lumped mass approximation are stated to provide a representation of both the bending and torsional effects.

Cables and other flexible pipes are found in many applications of civil, aerospace, and mechanical engineering. They are also commonly used in robotics, to bring energy to the actuators of a robotic arm. In ocean engineering, risers are used, for example, to convey fluids from the bottom of the sea up to the surface. In these applications, engineers need numerical models of nonlinear thin deformable structures in order to predict their motions and the internal stress for a given application. Hence, the need for numerical nonlinear beam models is still an intense subject of research. Among the most advanced finite element methods proposed for nonlinear beams, the geometrically exact approach initiated by Simo (Simo, 1985; Simo and Vu-Quoc, 1986, 1988) is probably one of the most efficient. This approach is based on the Cosserat assumption of rigid cross sections (Cosserat and Cosserat, 1909) and on Timoshenko internal kinematics (Timoshenko, 1921). However, when the "length/thickness" ratio of the beam becomes very high (i.e. when the structure is more of a rope or a cable than a beam, that is the rigidity to flexion is very low), the alternative internal kinematics of Kirchhoff and Clebsch (Love, 1944), are more appropiate as is done in ocean enginnering for the simulation of very long undersea cables (Burgess, 1993; Sun and Leonard, 1998) and in hydrodynamic or robotic problems (Boyer et al., 2011).

In fact, the dynamic modelling of marine cables has been studied extensively since the early 1960's for the analysis of mooring line tensions (Walton and Polacheck, 1960), and the positioning of towed vehicles (Chapman, 1984). However, the topic of low-tension cable dynamics is of more recent interest. Grosenbaugh et al. (Grosenbaugh et al., 1993) simulated the low tension tether motion of an underwater remotely operated vehicle (ROV) in two dimension using a finite difference approximation to the cable equations of motion and a representation of the tether bending stiffness. An alternative to the finite difference approach is the lumped mass strategy. In (Buckham and Nahon, 2001) the authors present and validate through experimentation, a lumped mass formulation for low tension cables that appends a bending stiffness model to a previously developed standard lumped mass formulation (Buckham et al., 2003; Driscoll et al., 2000). An advantage of the lumped mass method is the ease in coupling the formulation to the other numerical models, specifically to nonlinear vehicle models (Lambert et al., 2003).

There are two drawbacks to the existing low-tension lumped mass formulation: it needs small

linear elements to capture curvature variation, and there is currently no means for capturing the effects of a non-zero torsional stiffness. While existing model formulations (Burgess, 1992), make provision for the torsional stiffness in the continuous equation of motion, there has been no formulation where non-zero torsional effects have been considered in discrete analyses. Thus the role of torsional stiffness in the lumped mass approach remains without a mathematical proof. To address both shortcomings, a cubic element type is introduced by (Buckham et al., 2004) and equations of motion for the continuous cable are discretized using this higher order element.

The latter work develops a finite element cable model based on a third-order element with a reduced-order state vector. Following the developments of Garret (Garret, 1982) and Nordgren (Nordgren, 1974, 1982), the nonlinear equations of motion for the continuous tether in terms of an inertial frame of refererence using the Frenet equations, are developed. Finally, it will be shown that our particular choice of the finite element allows the assembled system of equations to be reduced into a system that has the same dimension as the simpler linear lumped parameter model, but yet mantains an accurate and complex representation of the higher order bending and torsional effects.

In general, finite element (FE) analysis of dynamic nonlinear deformations of solids and structures can be rather expensive, especially in situations when one requires many repeated trials, as often happens in design and control applications and uncertanty quantification. Model order reduction (MOR) seeks to reduce the computational complexity and computational time of large-scale dynamical systems by approximations of much lower dimension that can produce nearly the same input/output response characteristics. It is a very powerful technique that is used to deal with the increasing complexity of dynamic systems.

Originally, MOR was developed in the area of systems and control theory, which studies properties of dynamical systems in application for reducing their complexity, while preserving their input-output behavior as much as possible. The fundamental methods in the area of MOR were published in the eighties and nineties of the last century. In more recent years a lot of research has been done in the area of the MOR, and nowadays it is a flourishing field of research, both in systems and control theory and in numerical analysis. Consequently a large variety of methods is available.

Although there are different ways of approximating input-output systems, there is a unifying feature of the approximation methods: projection in an appropiate finite dimension subspace. Methods based on this concept truncate the solution of the original system in an appropriate basis, by projecting the original system onto a low-dimensional subspace.

In this work, we use a method known as Proper Orthogonal Decomposition (POD), which has been widely discussed in the literature during the last decades. The original concept goes back to Pearson (Pearson, 1901). The method is also known as Karhunen-Loève decomposition (Karhunen, 1946; Loève, 1946) or principal component analysis (Hoetelling, 1935). Further names are factor analysis or total least-squares estimation depending on the applications and certain conditions. It provides an optimally ordered, orthonormal basis in the least-squares sense for a given set of theoretical, experimental or computational data (Algazi and Sakrison, 1969). Reduced order models or surrogate models are then obtained by truncating this optimal basis. Clearly, the choice of the data set plays a crucial role and relies either on guesswork, intuition or simulations. Most prominent is the method of snapshots introduced by Sirovich (Sirovich, 1987). Here, the data set is chosen as time snapshots containing the spatial distribution of a numerical simulation at certain time instances reflecting the system dynamics. As an *a posteriori* data dependent method, it does not need *a priori* knowledge of the system behaviour

and can also be used to analyze patterns in data. In combination with Galerkin projection, it provides a powerful tool to derive surrogate models for high-dimensional or even infinite dimensional dynamical systems, since the subspace is composed of basis functions inheriting already special characteristics of the overall solution. This is in contrast to standard finite element discretizations where the choice of the basis functions is in general unrelated with the system dynamics.

The main advantage of POD lies in the fact that it requires only standard matrix computations, despite of its application to nonlinear problems. Although projecting only onto linear or affine subspaces, the overall nonlinear dynamics is preserved, since the surrogate model will still be nonlinear. Nevertheless, it is computationally more convenient than to project the dynamics onto a curved manifold (Rathinam and Petzold, 2003).

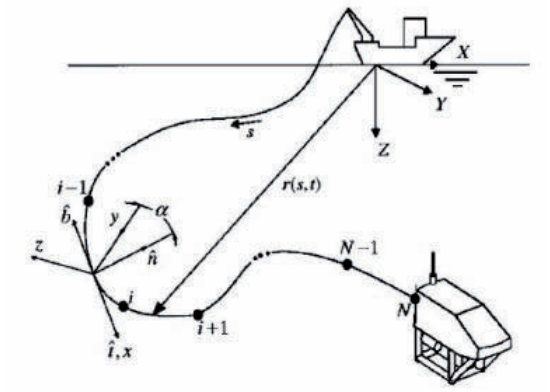

Figure 1: Schematic representation of the coordinate systems, the Frenet and body-fixed frames (Buckham et al., 2004).

2 MODEL STATEMENT AND EQUATIONS OF MOTION

In order to create a numerical model that includes the desired bending and torsional effects, it is necessary to derive the dynamic equations for a continuous cable considering the tortuous space curve, or profile, that the strained cable centerline attains in three-dimensional space. The formulation of the three-dimensional dynamics equations for a continuous cable has been discussed extensively in the existing literature. In general, the cable is modelled as a slender flexible rod under environmental, gravitational and buoyancy forces. Of particular relevance to this work was Nordgren's presentations (Nordgren, 1974) of the vector equations of motion for a continuos cable (Figs. 1 and 2) which are

$$\mathbf{F}' + \mathbf{q} = \left(\frac{1}{4}\pi d^2 \rho_c \mathbf{I}\right) \ddot{\mathbf{r}} \tag{1}$$

$$\mathbf{M}' + \mathbf{r}' \times \mathbf{F} + \mathbf{m} = \mathbf{0} \tag{2}$$

where ρ_c is the density of the cable, d is the diameter of the cable, $\mathbf{r}(s,t)$ is a position vector describing the space curve formed by the center line of the cable, $\mathbf{q}$ is the vector of applied forces per unit length, $\mathbf{m}$ represents the applied moment per unit length, $\mathbf{F}$ is the vector of internal forces, $\mathbf{M}$ is the vector of internal moments, $\mathbf{I}$ is a 3×3 identity matrix, $(')$ denotes differentiation with respecto to s, the unstretched curvilinear coordinate along the cable, and $(\dot{})$ denotes differentiation with respect to time t. We express $\mathbf{r}(s,t)$ in terms of an inertial frame

of reference (X, Y, Z), where X and Y point in perpendicular horizontal directions, and Z is aligned with the gravity direction. The rotational inertia of the cable is considered to be much smaller than the other terms of Eq. (1) and is thus neglected (Burgess, 1993). The dynamic equations are formulated using two local frames of reference, the Frenet frame and a frame of reference oriented with the principal axes of the cable, see Figure 1.

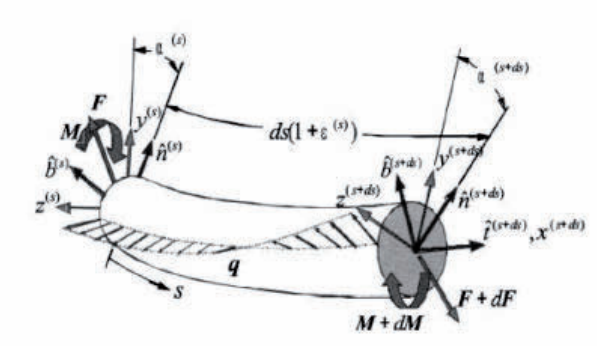

Figure 2: View of a differential segment of the cable(Buckham et al., 2004).

The Frenet frame $(\hat{\mathbf{t}}, \hat{\mathbf{n}}, \hat{\mathbf{b}})$ is oriented with the space curve formed by $\mathbf{r}(s,t)$. As the curve $\mathbf{r}(s,t)$ is traced, the changing orientation of the Frenet frame is quantified by two parameters: the curvature κ, and the torsion γ. Assuming the strain $\epsilon \ll 1$, the basis unit vectors are defined as: $\hat{\mathbf{t}} = \mathbf{r}'$, $\hat{\mathbf{n}} = \mathbf{r}''/\kappa$, and $\hat{\mathbf{b}} = (\mathbf{r}' \times \mathbf{r}'')\kappa$ and their gradients are defined as $\hat{\mathbf{t}}' = \kappa\hat{\mathbf{n}}$, $\hat{\mathbf{n}}' = -\gamma\hat{\mathbf{b}} - \kappa\hat{\mathbf{t}}$, and $\hat{\mathbf{b}}' = \gamma\hat{\mathbf{n}}$. The curvature, κ, denotes the bend of the cable within an osculating plane that is formed by $\hat{\mathbf{t}}$ and $\hat{\mathbf{n}}$ at the considered point. Both κ and γ are defined in terms of the spatial derivatives of the space curve:

$$\kappa = (\mathbf{r}'' \cdot \mathbf{r}'')^{1/2}$$
$$\gamma = \frac{\mathbf{r}' \cdot (\mathbf{r}'' \times \mathbf{r}''')}{\kappa^2}$$

The torsion of the curve γ is the spatial rate of change of the osculating plane orientation about the tangent vector, and consequently the orientation of the bend, about the tangent vector, $\hat{\mathbf{t}}$. As such, the torsion represents the twist experienced within the cable due to the shape of the cable profile. However, when the twist of the cable is considered, one recognizes that torsional couples applied at the boundaries of a cable section create an additional angular displacement, α (the torsion deformation). Thus, we introduce the body fixed reference frame (x, y, z) which remains aligned with the principal axes of the cross section, as shown in Figures 1 and 2, and is separated from the Frenet frame by an angle α about the tangent direction.

As discussed by Love, the internal moment, $\mathbf{M}$, generated at any point within the cable is proportional to the curvature and the twist observed at the point (Love, 1944):

$$\mathbf{M} = EI\kappa\hat{\mathbf{b}} + GJ\tau\hat{\mathbf{t}} \tag{3}$$

where E and G are the elastic and shear modulus, I is the area moment of inertia and J is the polar moment of inertia. The overall twist τ, of the cable at the point is given by

$$\tau = \gamma + \alpha' \tag{4}$$

Following (Garret, 1982) and (Nordgren, 1974), and assuming that there are no external moments applied between the cable boundaries ($\mathbf{m} = \mathbf{0}$), Eq. (3) is substituted into Eq. (2) to produce a definition for the vector of internal forces at any location along the cable

$$\mathbf{F} = T\hat{\mathbf{t}} - EI\kappa'\hat{\mathbf{n}} - EI\kappa\gamma\hat{\mathbf{b}} + GJ\tau\kappa\hat{\mathbf{b}}. \tag{5}$$

where T is defined in Eq (8), and the spatial derivative κ' is a nonlinear function of the spatial coordinate s, which complicates the finite element procedure that will be used. The second term on the right-hand side of Eq.(5) can be expressed as

$$EI\kappa'\hat{\mathbf{n}} = (EI\kappa\hat{\mathbf{n}})' - EI\kappa\gamma\hat{\mathbf{b}} + EI\kappa^2\hat{\mathbf{t}} \tag{6}$$

which allow the elimination of κ' in Eq. (5). Thus, subsituting Eq. (6) into Eq. (5) yields

$$\mathbf{F} = -(EI\kappa\hat{\mathbf{n}})' + (T - EI\kappa^2)\hat{\mathbf{t}} + GJ\tau\kappa\hat{\mathbf{b}} \tag{7}$$

where the term $-EI\kappa^2$ is included to cancel the spurious component of the internal force induced when considering the tangential component due to changing of $\hat{\mathbf{n}}$. The internal force, T, is defined using the constitutive relationship (a visco-elastic material)

$$T = EA\epsilon + C_{ID}\dot{\epsilon}, \qquad \epsilon = [(\mathbf{r}' \cdot \mathbf{r}')^{1/2} - 1] \tag{8}$$

where ϵ is the strain and C_{ID} is an internal viscous damping coefficient. This simple viscous damping model is used to represent the dissipation of energy within the cable via friction between the layers of conductors, armor, and polymer coatings of a typical cable. Equation (7) defines the internal force as an explicit function of the cable's elastic deformation as defined by the axial strain, curvature, and twist. Substituiting Eq. (7) into Eq. (1) reduces the two original vector equations of motion to a single vector equation that defines the translational motion in terms of these three elastic deformations, and a scalar constraint equation that defines the variation of the twist along the cable:

$$-(EI\mathbf{r}'')'' + [(T - EI\kappa^2)\mathbf{r}']' + [GJ\tau(\mathbf{r}' \times \mathbf{r}'')]' + \mathbf{q} = \left(\frac{1}{4}\pi d^2\rho_c\mathbf{I}\right)\ddot{\mathbf{r}} \tag{9}$$

$$(GJ\tau)' = 0. \tag{10}$$

In this work, the applied force vector $\mathbf{q}$ consists of the distributed weight and buoyancy, but can easily include hydrodynamic force, which can be defined using the well-known Morison's approximation. Since the Keulegan-Carpenter number of ocean cables is always very large, Morison's approximation is appropiate.

3 FINITE ELEMENT DISCRETIZATION

In the discretization process it is necessary to find a suitable approximations to both $\mathbf{r}(s,t)$ and $\alpha(s,t)$. Applying a finite element approach, the cable is considered as a contiguous set of N cubic segments, or elements, which have the same physical properties as the continuous cable. The trial solution $\mathbf{r}_i$ and α_i, defines the state of the i^{th} cable element extending between the nodes $i-1$ and i of the discrete cable. The shape of the element, $\mathbf{r}_i$, is defined in terms of the position and curvature vectors observed at the $i-1$ and i^{th} node points:

$$\begin{aligned}&\mathbf{r}(s,t) : s \in [s^{(i-1)}, s^{(i)}] \approx \mathbf{r}_i,\\ &\mathbf{r}_i = \mathbf{r}^{(i-1)}\phi_{i,1}(s) + \mathbf{r}''^{(i-1)}\phi_{i,2}(s) + \mathbf{r}^{(i)}\phi_{i,3}(s) + \mathbf{r}''^{(i)}\phi_{i,4}(s)\end{aligned} \tag{11}$$

As is discussed in detail in (Buckham et al., 2004), the element is a twisted cubic spline. The element shows a $\mathcal{C}^2(s)$, or second order, continuity across the node points to reflect the continuity expected in the curvature. The element is a superposition of a linear combination of the node points and a cubic refinement that interpolates the node curvature vectors.The shape functions are given by:

$$\begin{aligned} \phi_{i,1} &= \frac{s_i - s}{L_e}, \qquad & \phi_{i,2} &= \frac{1}{6}\left(\phi_{i,1}^3 - \phi_{i,1}\right) L_e^2 \\ \phi_{i,3} &= \frac{s - s_{i-1}}{L_e}, \qquad & \phi_{i,4} &= \frac{1}{6}\left(\phi_{i,3}^3 - \phi_{i,3}\right) L_e^2 \end{aligned} \tag{12}$$

where L_e is the length of the discrete cable elements. The specification of the $\mathcal{C}^2(s)$ continuity produces a system of tridiagonal linear equations that allow the curvature to be calculated from the node positions at any instant in the simulation. The element type thus minimizes the state variables required to define the cable shape at any time - the six position variables of the element node points. The trial solution is completed by modelling the torsional deformation within the element, α_i, as a linearly varying quantity between the node points:

$$\alpha_i = \alpha_{i-1}\phi_{i,1}(s) + \alpha_i\phi_{i,3}(s) \tag{13}$$

The optimum coefficients of the two polynomials are obtained through the application of Galerkin's criterion over the domain of the general element i^{th} element. The evaluation of the Galerkin residuals is described in (Buckham et al., 2004), including the various representations for the variation of the enviromental and internal effects over the element. The results of this procedure are the element equations given by:

$$\left([\mathbf{K}_B]_i + [\mathbf{K}_A]_i + [\mathbf{K}_\tau]_i\right)\mathbf{X}_i + \mathbf{W}_i + \mathbf{H}_i + \mathbf{B}_i = [\mathbf{M_e}]_i\ddot{\mathbf{X}}_i \tag{14}$$

and,

$$\frac{GJ}{L_e}\begin{bmatrix} 1 & -1 \\ -1 & 1 \end{bmatrix}\begin{Bmatrix} \alpha_{i-1} \\ \alpha_i \end{Bmatrix} = GJ\begin{Bmatrix} \gamma_{i-1/2} \\ -\gamma_{i-1/2} \end{Bmatrix} + \begin{Bmatrix} -GJ\tau_i^{i-1} \\ GJ\tau_i^i \end{Bmatrix} \tag{15}$$

where the boundary terms $GJ\tau_i^{i-1}$ and $GJ\tau_i^i$ represent the internal restoring torque at the boundaries of the element.

The 12×12 system matrices $[\mathbf{K}_B]_i$, $[\mathbf{K}_A]_i$ and $[\mathbf{K}_\tau]_i$ embody generalized bending, axial and torsional forces, respectively, that are applied at the element nodes and result from the curvature, axial strain and twist experienced throughout the cable element. The generalized load vectors $\mathbf{W}_i$, $\mathbf{H}_i$ and $\mathbf{B}_i$ define de gravitational, hydrodynamic, and applied forces respectively, and the 12×1 vector, $\mathbf{X}_i = \left\{\mathbf{r}_{i-1}^T, \mathbf{r}_{i-1}'^T, \mathbf{r}_i^T, \mathbf{r}_i'^T\right\}^T$, defines the element trial solution, given in Eq.(11).

The symmetric element mass matrix, $[\mathbf{M}_e]_i$ is reduced to a lumped mass matrix. This reduction effectively redistributes the cable mass such that it is concentrated at the node locations. A consequence of this reduction is the elimination of the time derivatives of the curvature vectors from the right hand side of Eq.(14) which reflects the fact that changes in the cubic element shape of the element, caused by changing curvature at the element end nodes, do not accelerate any cable mass. Through the lumped mass approximation, Eq.(14) is reduced to a system of 6 equations (rather than 12) by premultiplying both sides by

$$\mathbf{P} = \begin{bmatrix} \mathbf{1} & \frac{1}{L_e}\mathbf{1} & \mathbf{0} & \mathbf{0} \\ \mathbf{0} & \mathbf{0} & \mathbf{1} & \frac{1}{L_e}\mathbf{1} \end{bmatrix} \tag{16}$$

where $\mathbf{1}$ is a 3×3 identity matrix. The pre-multiplication by $\mathbf{P}$ transforms the 12×12 system matrices and 12×1 load vectors into 6×12 system matrices and 6×1 quantities, respectively, that given the temporal change of the element's 6 state variables, the node positions. It is these reduced matrices and vectors that are the basis for the model assembly.

Applying the element Eqs. (14) and (15) for each node in the concatenation of elements, $0 \leq i \leq N$, a global system of equations of motion and twist constraints are produced. The form of the assembled equations is

$$\ddot{\mathbf{R}} = \mathbf{F}(t, \mathbf{R}, \dot{\mathbf{R}}) \tag{17}$$

where $\mathbf{R} = \left\{ \mathbf{r}^{(0)T}, \mathbf{r}^{(1)T}, \ldots, \mathbf{r}^{(N)T} \right\}^T$.

Equation (17) is a series of $3(N+1)$ second order differential equations. Given a set of initial conditions $\mathbf{R_0} = \mathbf{R}(t=0)$ and $\dot{\mathbf{R}}_\mathbf{0} = \dot{\mathbf{R}}(t=0)$ the model can evolve in time by the specification of boundary conditions and the provision of a suitable integration routine.

4 MODEL ORDER REDUCTION

The main idea of model reduction is to find a spatial repesentation of the primary variable $\mathbf{R}$, which would ensure the response of the full and reduced models to be close in certain sense, and which would be at the same time much faster than the full FE model. In other words, we would like to find a representation minimizing the number of degrees of freedom needed in the computation to reach a certain error level (measured with respect to the full FE model). Most reduction methods for nonlinear dynamic finite element analysis are based on projection onto a finite dimension subspace. The original motion given by the position vector $\mathbf{R}$ is projected onto a subspace where the projection is described by

$$\mathbf{R}(t) = \mathbf{Q}\,\mathbf{q}(t) \tag{18}$$

where $\mathbf{q}(t) \in \mathbb{R}^k \subset \mathbb{R}^n$ is the motion in the subspace. The columns of the transformation matrix $\mathbf{Q} \in \mathbb{R}^{n \times k}$ are the basis vectors, which span the subspace. Inserting Eq. (18) into the dynamic equilibrium (Eq. 17) and pre-multiplying by $\mathbf{Q}^T$ (that is, projecting in the subspace spanned by) yields the reduced system

$$\mathbf{Q}^T\mathbf{Q}\ddot{\mathbf{q}}(t) = \mathbf{Q}^T\mathbf{F}(t, \mathbf{Q}\,\mathbf{q}(t), \mathbf{Q}\,\dot{\mathbf{q}}(t)) \tag{19}$$

The choice of the reduced basis clearly affects the quality of approximation. The techniques for constructing the reduced basis use a common observation that, for a particular system, the solution space is often attracted to a low-dimensional manifold. Among the various techniques for obtaining a reduced basis, Proper Orthogonal Decomposition constructs a set of global basis functions from a singular value decomposition (SVD) of *snapshots*, which are discrete samples of trajectories associated with a particular set of boundary conditions and inputs. This basis is *optimal* in the sense that a certain approximation error concerning the snapshots is minimized. Thus, the space spanned by the basis from POD often gives an excellent low-dimensional approximation. Once the reduced model has been constructed from this reduced basis, it may be used to obtain approximate solutions for a variety of initial conditions and parameter settings, provided the set of samples is rich enough. This empirically derived basis is clearly dependent on the sampling procedure.

5 PROPER ORTHOGONAL DECOMPOSITION (POD)

POD is a method for constructing a low-dimensional approximation representation of a subspace in a Hilbert space. It is essentially the same as the SVD in a finite-dimensional space or in Euclidean space. It efficiently extracts the basis elements that contain characteristics of the space of expected solutions of the PDE. Sometimes, like in our case of study is best to find an affine subspace as opposed to linear subspace. This requires us first to find the mean value of the data points. The POD basis in Euclidean space may be specified formally as follows.

Let $\{\mathbf{y}_1, \ldots, \mathbf{y}_m\} \subset \mathbb{R}^n$ be a set of centered (with respect to the mean) snapshots (recall that snapshots are samples of trajectories):

$$\mathbf{y}_i = \mathbf{R}_i - \overline{\mathbf{R}} \tag{20}$$

where $\mathbf{y}_i$ is the i-th centered snapshot, $\mathbf{R}_i$ is the i-th snapshot obtained using the Finite Element model and $\overline{\mathbf{R}}$ is the mean trajectory. Let $\mathcal{Y} = span\{\mathbf{y}_1, \ldots, \mathbf{y}_m\} \subset \mathbb{R}^n$ and r is the rank of $\mathcal{Y}$. A POD basis of dimension $k < r$ is a set of orthonormal vectors $\{\phi\}_{i=1}^k \subset \mathbb{R}^n$ whose linear span best approximates the space $\mathcal{Y}$. The basis set $\{\phi\}_{i=1}^k$ solves the minimization problem

$$\min_{\{\phi\}_{i=1}^k} \sum_{j=1}^m \left|\left| \mathbf{y}_j - \sum_{i=1}^k (\mathbf{y}_j^T \phi_i)\phi_i \right|\right|_2^2 \tag{21}$$

with

$$\phi_i^T \phi_j = \delta_{ij} = \begin{cases} 1 & \text{if} \quad i = 1\,, \\ 0 & \text{if} \quad i \neq j, \end{cases} \qquad i, j = 1, \ldots, k.$$

It is well known that the solution to Eq. (21) is provided by the set of the left singular vectors of the *snapshots matrix* $\mathbf{Y} = [\mathbf{y}_1, \ldots, \mathbf{y}_m] \in \mathbb{R}^{n \times m}$. In particular, suppose that the SVD of $\mathbf{Y}$ is

$$\mathbf{Y} = \mathbf{V}\mathbf{\Sigma}\mathbf{W}^T, \tag{22}$$

where $\mathbf{V} = [\mathbf{v}_1, \ldots, \mathbf{v}_n] \in \mathbb{R}^{n \times n}$ and $\mathbf{W} = [\mathbf{w}_1, \ldots, \mathbf{w}_m] \in \mathbb{R}^{m \times m}$ are orthogonal and $\Sigma \in \mathbb{R}^{n \times m}$ contains the singular values on its diagonal $(\sigma_1, \ldots, \sigma_r)$ with $\sigma_1 \geq \sigma_2 \geq \ldots \geq \sigma_r > 0$. The rank of $\mathbf{Y}$ is $r \leq \min(n, m)$. Then the POD basis or the optimal solution of Eq.(21) is $\{\mathbf{v}_i\}_{i=1}^k$. The minimum 2-norm error from approximating the snapshots using the POD basis is then given by

$$\sum_{j=1}^m \left|\left| \mathbf{y}_j - \sum_{i=1}^k (\mathbf{y}_j^T \phi_i)\phi_i \right|\right|_2^2 = \sum_{i=k+1}^r \sigma_i^2. \tag{23}$$

We refer the reader to (Kunisch and Volkwein, 2008) for more details on the POD basis in general Hilbert space.

The choice of the snapshot ensemble is a crucial factor in constructing a POD basis. This choice can greatly affect the approximation of the original solution space, but is a separate issue and will not be discussed here. POD is a popular approach because it works well in many applications and often provides an excellent reduced basis. However, as discussed in the introduction, when POD is used in conjunction with the Galerkin projection, effective dimension reduction is usually limited to the linear terms or low-order polynomial nonlinearities. Systems with general nonlinearities need aditional treatment (Chaturantabut and Sorensen, 2010).

6 NUMERICAL ILLUSTRATION

The dynamical response of a cable was analyzed by means of the above proposed finite element approach. The total length of the cable is $L = 47$m. The cable was supposed fixed at the left end with its right end subjected to prescribed motions with the following cosine functions

$$\begin{aligned} X(L,t) &= A_1 + a_1 \cos(\omega_1 t), \\ Y(L,t) &= A_2 + a_2 \cos(\omega_2 t), \\ Z(L,t) &= A_3 + a_3 \cos(\omega_3 t). \end{aligned} \tag{24}$$

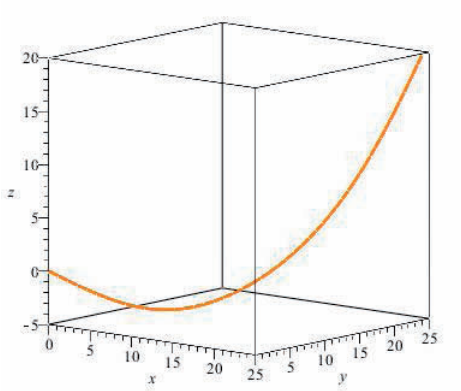

Figure 3: Initial geometric configuration of the cable.

The following mechanical and geometrical properties were adopted: $\rho_c = 7850$ kg/m^3 (density), $E = 2.1 \times 10^{11}$ N/m^2 (Young Modulus), $d = 2.85 \times 10^{-2}$ m (diameter), $C_D = 0$ (internal viscous damping). In all cases, the (unstretched) condition at initial instant was adopted to be the static solution of an inextensible cable subjected to selfweight (catenary solution) with ends coordinates $(0, 0, 0)$ and $(40, 40, 20)$ (see Fig. 3).

6.1 Example 1

In order to check the performance of the finite element model, a series of simulations with different number of elements were run. The parameters that define the prescribed motions at the end of the cable at every instant of time were adopted as: $A_1 = A_2 = 26.16m$, $A_3 = 18$m, $a_1 = a_2 = 2.12$m, $a_3 = 2$m, $\omega_1 = \omega_2 = 0.5$ rad/s, $\omega_3 = 0.75$ rad/s. Figure (4) depicts the motion of the chain by superposing different positions, for a total time of 10 seconds, and also their projections onto the xy plane where it can be observed that the cable stays in the same vertical plane at every instant, as expected for an initial configuration and a load contained in the same plane.

Since in this example the cable is subjected to a relative low-speed motion, a comparison with a chain under the same action is now depicted. An algorithm that deals with the dynamic of chains modelled as concentrated point mass joined by springs, is reported in (Wilson et al., 2003). A 32 link chain was solved using this algorithm for a qualitative comparison with results from the present cable FEM formulation. Figure 5 shows the trajectory described by the middle point for both models. The point describes the trajectory more than once during the considered time which is reflected with various blue lines. In the two cases the same qualitative response was obtained.

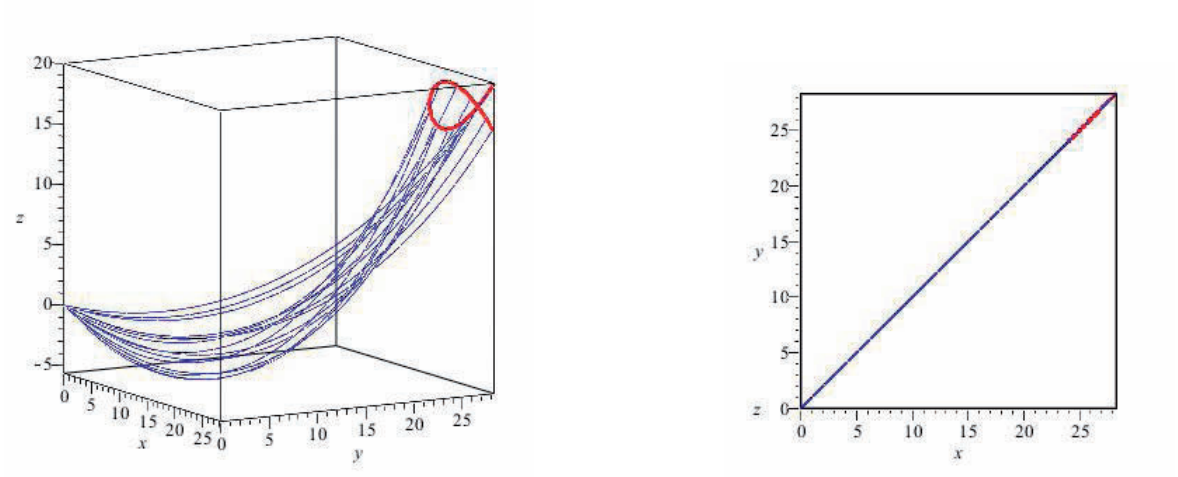

Figure 4: Left: snapshots of the cable motion at first 30 seconds and trajectory described by the end of the cable (red). FEM with 32 elements.Right: xy projection of snapshots

.

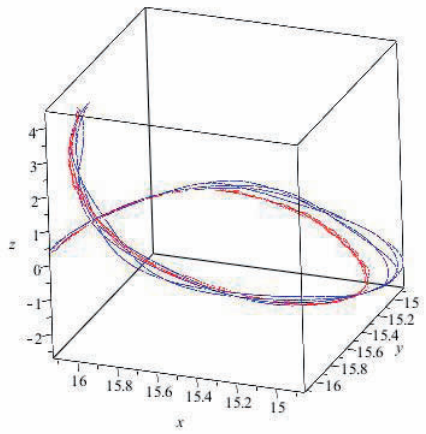

Figure 5: Trajectory described for the midle point form both models: present FEM formulation (blue) , concentrated mass and springs formulation (red). Total time 50s, 32 elements.

Now and in order to construct a reduced order model using POD, a FE simulation with 32 elements was run for a total time of 100 seconds from which the snapshots matrix was obtained (one snapshot every 0.1 seconds). Then, following the procedure detailed in Section 5 the POD basis was obtained to get the $\mathbf{Q}$ projection orthogonal matrix used to reduce the dimension (degrees of freedom) of the problem .The results obtained with the reduced FE using 5 and 6 eigenvectors (Proper Orthogonal Values, POMs) corresponding to the highest 5 or 6 eigenvalues (Proper Orthogonal Values, POVs), respectively, are depicted in Figure 6. It can be observed that adding the sixth POM achieves an adequate approximation.

It should be noted that the total time needed for a simulation with a reduced order model was significantly decreased compared with the full FE model. Some comments on the time reduction are included in the next example.

6.2 Example 2

The dynamics of the same cable is now analyzed but under a different motion and an angular displacement $\alpha(L,t)$ (torsional deformation) at the top right end. The following values were

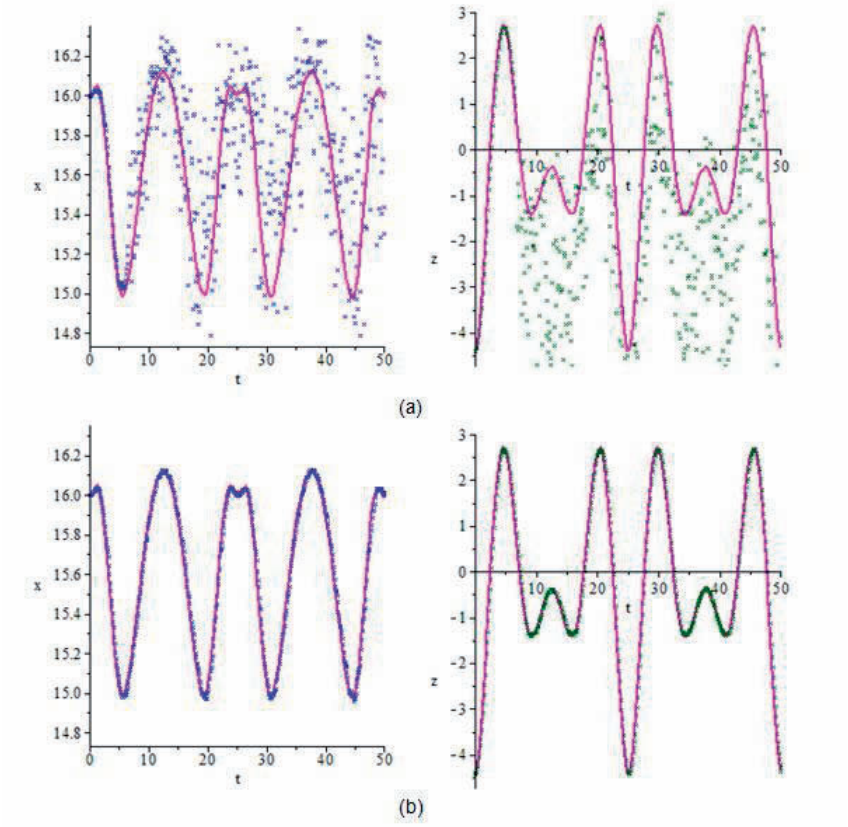

Figure 6: Example 1. Temporal variation of the center point of the cable. Left graphs: coordinate x vs. time. Right graphs: coordinate z vs. time. Fuchsia curve: FEM solution with 32 elements. Blue points: reduced order model solution with POD. a) 5 POMs, b) 6 POMs.

adopted: $A_1 = A_2 = 26.16m$, $A_3 = 18$m, $a_1 = a_2 = 2.12$m, $a_3 = 2$m, $\omega_1 = 0.5$rad/s, $\omega_2 = 0.75$rad/s, $\omega_3 = 0$rad/s, $\alpha(L,t) = \pi(1 - \cos(0.15t))$.Figure 7 shows the 3D trajectory of the central point at 50 seconds, found both with the FEM results (32 elements) and the reduced order model output (6 POMs).

The first 30 seconds snapshots are depicted in Figure 8 found with the FEM with 32 elements (left graph, blue line). The right plot shows the xy projections of the snapshots, from which the out-of-plane motion is apparent. Also, the prescribed motion at the right end is plotted in red line. It should be noted that the computational time for a 6 POMS reduced model takes the 30% of the time necessary to run the non-reduced model. This feature is desirable when, for instance, one performes quantification of uncertainties that require of a large number of realizations to achieve the statistical study.

The effect of the addition of POMs is clearly observed at Figure 9. The time history of the central point x coordinate was found for 6, 7, 8 and 9 eigenvectors (POMs). The number of POMs to approximate adequately the dynamics of the cable, appears to be 8 or 9. Finally, Figure 10 depicts the 3D trajectories found with the FEM (50 seconds, 32 elements) (left plot) and the same trajectory superimposed to the reduced order model one (9 POMs) at the right plot. Again, it is seen that the dynamics is appropriately approximated with a more efficient approach.

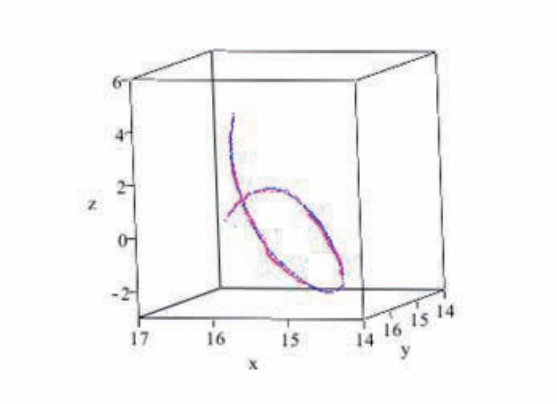

Figure 7: Example 2. Trajectory of the center point of the cable at 50 seconds. Fuchsia curve: FEM with 32 elements. Blue: reduced order model with 6 POMs.

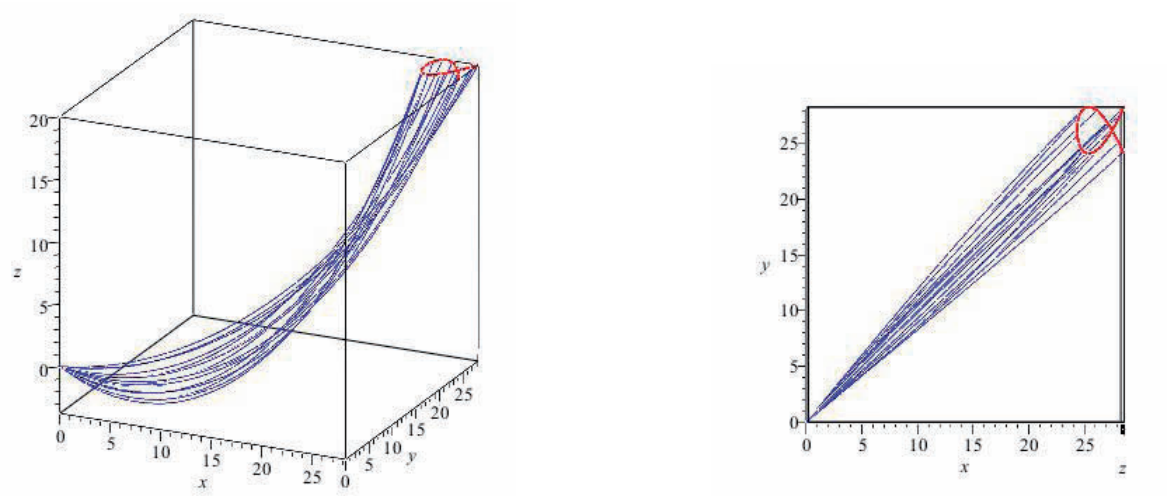

Figure 8: Example 2. First 30 seconds snapshots found with the FEM with 32 elements (left graph, blue line). xy projection of the snapshots (right graph, blue line). Prescribed displacement at right end (red line).

.

7 CONCLUSIONS

In this work, a finite element simulation of cables was shown to obtain a reduced order model by means of the projection method using Proper Orthogonal Decompositions (POD). A twisted cubic spline element form and a lumped mass approximation was adopted to provide a representation of both the bending and torsional effects. The nonlinear equations of motion for the continuous cable were developed in terms of an inertial frame of reference using the Frenet equations. The proper orthogonal modes, in conjunction with the Galerkin approach, by projecting the original system onto a low-dimensional subspace, was used for the construction of a lower-dimensional model that, as it was shown in the numerical examples, is very efficient with respect to the ones constructed with the typical finite elements basis. Computing POD requires only standard matrix computations, despite of its application to nonlinear problems. Although projecting only onto linear or affine subspaces, the overall nonlinear dynamics is preserved, since the surrogate model will still be nonlinear.

In the present study, the FEM models were run with larger times than the necessary ones in the reduced model. That is, the reduced model is an interpolation of the original one. Further

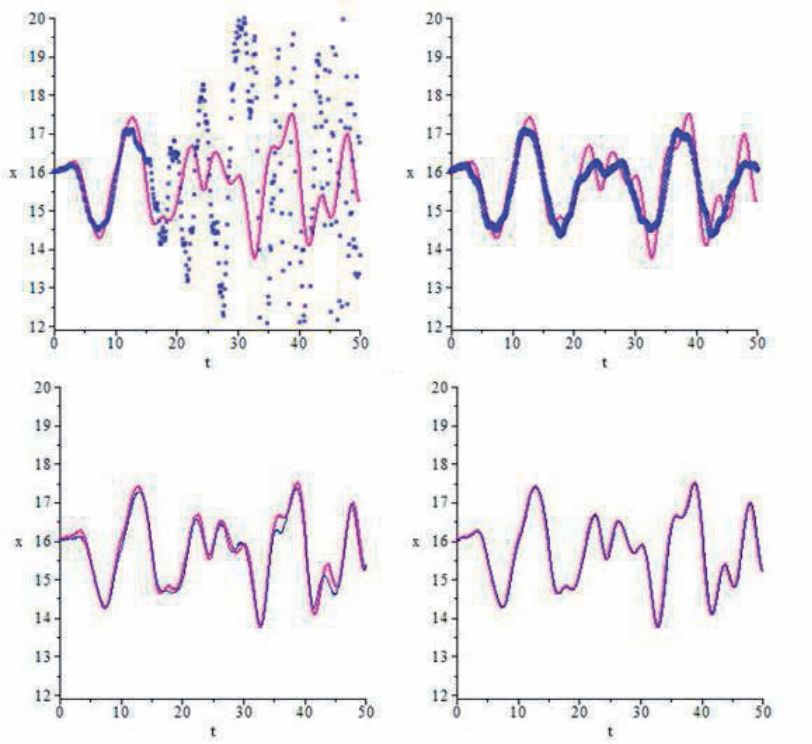

Figure 9: Time history of the x coordinate of the midle point: 6,7,8 y 9 eigenvectors.

studies are needed to obtain significant reduced models in ranges of times beyond the original interval. Regarding the boundary conditions, the POD depends on them and, so far, a new bases set has to be found for each case. However, the extension to other situations such as other initial conditions and parameter settings is possible provided the set of samples is rich enough (Chaturantabut and Sorensen, 2010).

It should be noted that in the presence of a general nonlinearity, the standard POD-Galerkin technique reduces dimensions in the sense that far fewer variables are present, but the complexity of evaluating the nonlinear term remains that of the original problem.

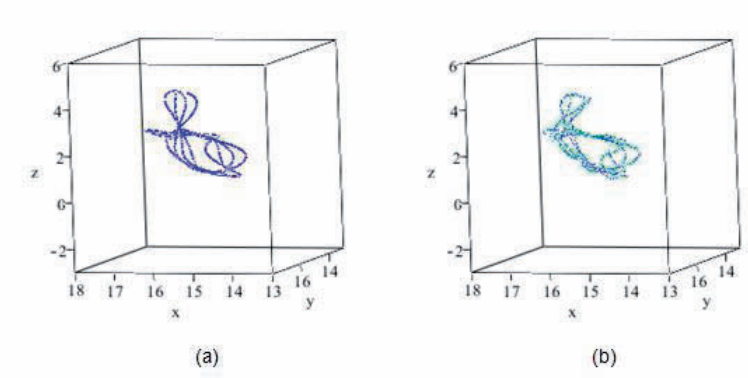

Figure 10: Example 2. Central point trajectory. FEM model: Simulation time of 50 seconds, 32 elements (left graph). FEM model (blue line) and reduced model with 9 POMs (green line).

8 ACKNOWLEDGEMENT

The authors are grateful to the financial support from CAPES, CNPq, and FAPERJ from Brasil, and FRCU-UTN, FRCon-UTN, SGCyT-UNS and CONICET from Argentina.

REFERENCES

Algazi V. and Sakrison D. On the optimality of the Karhunen-Loève expansion. *IEEE Trans. Information Theory*, 15:319–320, 1969.

Boyer F., De Nayer G., Leroyer A., and Visonneau M. Geometrically exact Kirchoff beam theory: Application to cable dynamics. *Journal of Computantional and Nonlinear Dynamics*, 6(4):41004/1–41004/14, 2011.

Buckham B., Driscoll F., and Nahon M. Development of a finite element cable model for use in low-tension dynamics simulation. *ASME Jounal of Applied Mechanics*, 71:476–485, 2004.

Buckham B. and Nahon M. Formulation and validation of a lumped mass model for low-tension rov tethers. *International Journal of Offshore and Polar Engineering*, 11(4):282–289, 2001.

Buckham B., Nahon M., Seto M., Zhao X., and Lambert C. Dynamics simulation of a towed underwater system: Part i model development. *Ocean Engineering*, 30(4):453–470, 2003.

Burgess J. Equations of motion of a submerged cable with bending stiffness. *Proceedings of the International Offshhore Mechanics and Arctic Engineering*, pages 283–290, 1992.

Burgess J. Bending stiffness in a simulation of undersea cable deployment. *International Journal of Offshore and Polar Engineering*, 3:197–204, 1993.

Chapman D. Towed cable behaviour during ship turning maneuvers. *Ocean Engineering*, 11(4):327–361, 1984.

Chaturantabut S. and Sorensen D. Nonlinear model reduction via discrete empirical interpolation. *Journal of Scientific Computing*, 32(5):2737–2764, 2010.

Cosserat E. and Cosserat F. *Théorie des corps d''eformables*. Hermann, 1909.

Driscoll F., Lueck R., and Nahon M. Development and validation of a lumped-mass dynamics model of a deep-sea rov system. *Applied Ocean Recearch*, 22(3):169–182, 2000.

Garret D. Dynamic analysis of slender rods. *ASME Journal of Energy Resources Technology*, 104:302–306, 1982.

Grosenbaugh M., Howell C., and Moxnes S. Simulating the dynamics of underwater vehicles with low tension tethers. *International Journal of Offshore and Polar Engineering*, 3(3):213–218, 1993.

Hoetelling H. Simplified calculation of principal component analysis. *Psychometrica*, 1:27–35, 1935.

Karhunen K. Zur spektraltheorie prozesse. *Annales Academiae Scientiarum Fennicae, Ser. A*, 34, 1946.

Kunisch K. and Volkwein S. Proper orthogonal decomposition for optimality systems. *Mathematical Modelling and Numerical Analysis*, 42(1):1–23, 2008.

Lambert C., M. N., Buckham B., and Seto M. Dynamics simulation of a towed underwater system: Part ii model validation and turn maneuver optimization. *Ocean Engineering*, 30(4):471–485, 2003.

Loève M. Fonctions aleatoire de second ordre. *Revue*, 48:195–206, 1946.

Love A. *A Treatise on the Mathematical Theory of Elasticity*. Dove, New York, 4th edition, 1944.

Nordgren R. On the computation of the motion of elastic rods. *ASME Jounal of Applied Mechanics*, 41:777–780, 1974.

Nordgren R. Dynamic analysis of marine risers with vortex excitation. *ASME Journal of Applied Mechanics*, 104:14–19, 1982.

Pearson K. On lines and planes of closest to points in space. *Philosophical Magazine*, 2:609–629, 1901.

Rathinam M. and Petzold L. A new look at proper orthogonal decomposition. *SIAM J. Numer. Anal.*, 41(5):1893–1925, 2003.

Simo J. A finite strain beam formulation. the three-dimensional dynamic problem. part i: Formulations and optimal parametrization. *Computational Methods in Applied Mechanics and Engineering*, 49:55–70, 1985.

Simo J. and Vu-Quoc L. A three dimensional finite strain rod model. part ii: Computational aspects. *Computational Methods in Applied Mechanics and Engineering*, 58:79–116, 1986.

Simo J. and Vu-Quoc L. On the dynamics in space of rods undergoing large motions - a geometricallly exact approach. *Computational Methods in Applied Mechanics and Engineering*, 66:125–161, 1988.

Sirovich L. Turbulence and the dynamics of coherent structures. i-iii. *Quarterly of applied mathematics*, 45(3):561–590, 1987.

Sun Y. and Leonard J. Dynamics of ocean cables with local low-tension regions. *IEEE Journal of Oceanic Engineering*, 25(6):443–463, 1998.

Timoshenko S. On the correction for shear of the differential equation for transverse vibrations of prismatic bars. *Philosophical Magazine Series*, 41:744–746, 1921.

Walton T. and Polacheck H. Calculation of transient motion of submerged cables. *Mathematics of Computation*, 14(69):27–46, 1960.

Wilson H., Turcotte L., and Halpern D. *Advanced mathematics and mechanics applications using MATLAB*. CRC press, 2003.